Psychophysiology, 40 (2003), 529–541. Blackwell Publishing Inc. Printed in the USA.

Optical coherence tomography: Technology and applications for neuroimaging

STEPHEN A. BOPPART

Department of Electrical and Computer Engineering, Bioengineering Program, and Beckman Institute for Advanced Science and Technology, College of Medicine, University of Illinois at Urbana–Champaign, Urbana, Illinois, USA

Abstract

Optical coherence tomography (OCT) is an emerging imaging technology with applications in biology, medicine, and materials investigations. Attractive features include high cellular-level resolution, real-time acquisition rates, and spectroscopic feature extraction in a compact noninvasive instrument. OCT can perform "optical biopsies" of tissue, producing images approaching the resolution of histology without having to resect and histologically process tissue specimens for characterization and diagnosis. This article will review several of the current technological developments in OCT. To illustrate the potential of this technology for neuroimaging, applications for imaging neural development, the neural retina, tumors of the central nervous system, and the microsurgical repair of peripheral nerves will be presented. This technology offers a potential investigative tool for addressing many of the present challenges in neuroimaging.

Descriptors: Imaging, Optics, Spectroscopy, Optical coherence tomography

In recent years, biomedical imaging technology has made rapid advances that enable the visualization, quantification, and monitoring of morphology and function. New technologies have pushed the limits of imaging from organ-level tissue morphology to cellular structures and even to molecular composition. In the fields of neuroscience and neural imaging, technologies such as computed tomography (CT), magnetic resonance imaging (MRI), positron emission tomography (PET), and diffusion optical imaging have enabled a wide range of investigations into the structure and function of the brain. Optical microscopy techniques, including light, confocal, and multiphoton imaging have provided researchers with the ability to understand complex interactions at the cellular level. Optical coherence tomography (OCT) is an emerging biomedical imaging technology that has been applied to a wide range of biological, medical, and materials investigations. OCT is analogous to ultrasound (US) B-mode imaging except reflections of near-infrared light are detected rather than sound. OCT offers noninvasive real-time, high-resolution imaging of cell and tissue microstructure deep within highly scattering tissues. Although OCT has been demonstrated in several areas of neuroimaging, the full potential for this technology has yet to be realized. This review will describe the principles of operation and the recent technological developments of OCT. To illustrate its applicability across many disciplines, applications to developmental neurobiology, retinal imaging, cell and tumor imaging, and image-guided surgery will be reviewed. By fully exploiting the unique capabilities of this technique, the potential exists for addressing many of the current technical imaging and visualization challenges in the fields of neuroscience and neural imaging.

OCT was developed in the early 1990s for the noninvasive imaging of biological tissue (Bouma & Tearney, 2001; Huang et al., 1991). The first application areas were in ophthalmology, where diagnostic imaging could be performed on the transparent structures of the anterior eye and the retina (Hee et al., 1995; Puliafito, Hee, Lin, et al., 1995; Puliafito, Hee, Schuman, & Fujimoto, 1995). OCT has been successfully applied across a wide range of subspecialty areas in ophthalmology because it can provide cross-sectional imaging with micron-scale resolution. Recent developments in this area have demonstrated retinal imaging at 3-μm resolution, permitting the differentiation of individual retinal layers in vivo (Drexler et al., 2001). Clinical studies have been performed with research and commercially available instruments (Humphrey OCT3, Zeiss Humphrey Instruments) to assess the application of OCT for a number of retinal diseases associated with diabetic retinopathy including macular edema and thinning of the retinal nerve fiber layer secondary to glaucoma (Bowd et al., 2001; Williams et al., 2002).

I thank my colleagues and my students for their contributions to this work and Sonya Chappell for her assistance in preparing the manuscript. Our current research in developing and applying the OCT technology would not be possible without the support and funding from the National Science Foundation (BES-0086696), the Whitaker Foundation, the National Aeronautics and Space Administration (NAS2-02057), the National Institutes of Health (NCI, NIBIB; 1 RO1 EB00108-1), and the Beckman Institute for Advanced Science and Technology. Additional information about the OCT technology can be found at http://nb.beckman.uiuc.edu/biophotonics.

Address reprint requests to: Stephen A. Boppart, M.D., Ph.D., Beckman Institute for Advanced Science and Technology, 405 N. Mathews Avenue, Urbana, IL 61801, USA. E-mail: boppart@uiuc.edu.

Because morphological changes often occur before the onset of physical symptoms in these diseases, OCT can provide a means for early detection. In addition, follow-up imaging can assess treatment effectiveness and recurrence of disease.

OCT systems using optical sources at longer wavelengths have enabled deep-tissue imaging in highly scattering soft tissues (Brezinski et al., 1996). To date, in vitro and in vivo imaging studies have been performed in many of the major systems of the human, including applications to cardiology (Brezinski, Tearney, Weissman, et al., 1997; Jang et al., 2002; Tearney et al., 1996), gastroenterology (Bouma, Tearney, Compton, & Nishioka, 2002; Das et al., 2001; Izatt, Kulkarni, Wang, Kobayashi, & Sivak, 1996; Li et al., 2001; Tearney et al., 1997a), urology (Tearney et al., 1997b; Zagaynova et al., 2001), dermatology (Podoleanu, Rogers, Jackson, & Dunne, 2000; Schmitt, Yadlowsky, & Bonner, 1995), and dentistry (Colston et al., 1998), to name only a few. OCT has been used for tumor diagnostics in a range of organ systems, including the brain (Boppart, Brezinski, Pitris, & Fujimoto, 1998; Fujimoto, Pitris, Boppart, & Brezinski, 2000). In the biological sciences, OCT has been demonstrated for microscopy applications in developmental biology, including developmental neurobiology (Boppart, Brezinski, Bouma, Tearney, & Fujimoto, 1996; Boppart, Brezinski, Tearney, Bouma, & Fujimoto, 1996; Boppart, Tearney, et al., 1997; Rollins, Kulkarni, Yazdanfar, Ungarunyawee, & Izatt, 1998). The small developmental biology animal models commonly used in this field, such as *Drosophila* (fruit fly), *Brachydanio rerio* (zebra fish), and *Xenopus laevis* (African frog), have rapidly developing morphology on a size scale that is matched to the high-resolution imaging capabilities of OCT. Improvements in OCT imaging resolution have permitted the visualization of individual cells and cellular processes such as mitosis and cell migration (Boppart, Bouma, Pitris, Southern, et al., 1998). OCT has been used to track the in vivo migration of neural crest cells (Boppart, Bouma, Pitris, Southern, et al., 1998), which could be an important technique for further investigations in the field of developmental neuroscience.

Nonbiological applications for OCT have included the nondestructive evaluation of materials including polymers, ceramics, and coatings (Duncan, Bashkansky, & Reintjes, 1998; Xu, Pudavar, Prasad, & Dickensheets, 1999). The optical ranging capabilities of OCT have been used to optically read out digital data from multilayer optical disks (Chinn & Swanson, 1996), offering a potential solution to current data storage limitations.

Principles of Operation

OCT performs optical ranging in biological tissue. Optical ranging has routinely been used in the telecommunications industry for locating faults or defects in optical fibers that comprise an optical communications network (Takada, Yokohama, Chida, & Noda, 1987). Faults in fiber produce a partial or complete reflection of incident optical pulses. By sending optical pulses through the optical fiber, faults can be detected by measuring the time delay between the original and reflected pulse. Analogous to optical ranging in fibers, optical ranging can be performed in biological tissue because every interface (where there is a change in the optical index of refraction) will reflect a portion of the incident optical beam. The first applications in biological samples included one-dimensional optical ranging in the eye to determine the location of different ocular structures (Fercher, Mengedoht, & Werner, 1988; Hitzenberger, 1991). The image formed in OCT represents a series of adjacent one-dimensional optical ranging scans assembled to produce a two-dimensional cross-sectional image.

In contrast to US, which performs ranging by measuring the time delay of a reflected sound wave, the velocity of light is extremely high and therefore the time delay of reflected light cannot be measured directly. Instead, interferometric detection techniques must be used. One method for measuring the time delay is to use low-coherence interferometry or optical coherence domain reflectometry. Low-coherence interferometry is performed using a Michelson type interferometer (Figure 1). Light from the optical source is split in half by a beam splitter with half sent down the reference arm and half sent down the sample arm of the interferometer. Reflections from the reference arm mirror and from within the sample are recombined by the beam splitter and sent to the detector. The electrical signal from the photodetector is bandpass filtered, demodulated, digitized, and stored on a computer. Because low-coherence light is used, interference of the light only occurs when the optical path lengths are matched between the two arms of the interferometer. Hence, the position of the reference arm mirror determines the depth in the sample from which the magnitude of the reflection is measured. By scanning the reference arm mirror, a single axial depth scan of reflection data is acquired from the sample. The position of the incident beam on the tissue is then scanned in the transverse direction and multiple axial measurements are performed to generate a two-, three-, or four-dimensional data array that represents the optical backscattering from the tissue (Figure 2). The intensity (magnitude) of the reflections is assigned a false-color or gray-scale and displayed as an OCT image. The interferometer can be implemented with a fiber-optic

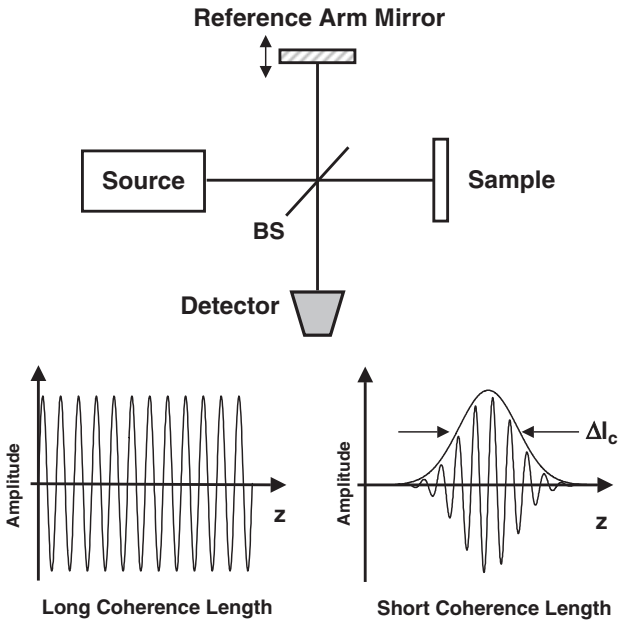

Figure 1. Schematic illustrating the concept of low coherence interferometry. Using a short coherence length light source and a Michelson-type interferometer, interference fringes are observed only when the path lengths of the two interferometer arms are matched to within the coherence length (Δl_c) of the light source.

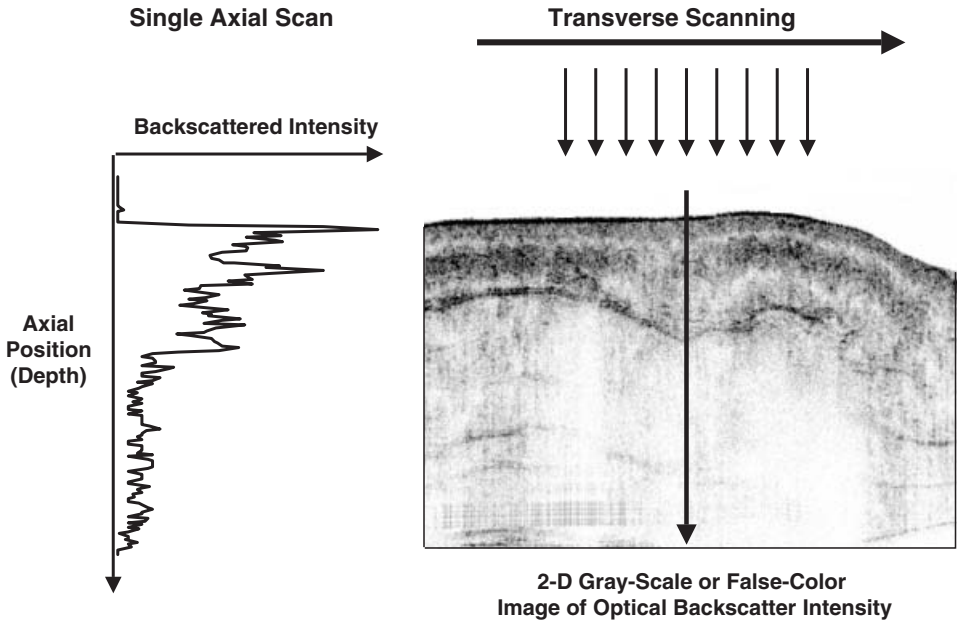

Figure 2. An OCT image is based on the spatial localization of variations in optical backscatter from within a specimen. Images are acquired by performing axial measurements of optical backscatter at different transverse positions on the specimen and displaying the resulting two-dimensional data set as a gray-scale or false-color image.

coupler, and different modular beam-scanning systems can be used to deliver the imaging beam to the tissue, including microscopes (Beaurepaire, Moreauz, Amblard, & Mertz, 1999), fiber-optic catheters and endoscopes (Feidchtein et al., 1998; Pan, Xie, & Fedder, 2001; Tearney, Brezinski, Bouma, et al., 1997), and hand-held imaging probes (Boppart, Bouma, et al., 1997; Li, Chudoba, Ko, Pitris, & Fujimoto, 2000). The use of fiber optics enables OCT systems to be compact and portable, roughly the size of a small cart (Figure 3).

The important parameters for characterizing an OCT system are the imaging resolution, the signal-to-noise ratio (SNR), the depth of imaging penetration, and the image acquisition rate. In contrast to conventional microscopy, the axial (depth) resolution and the transverse (lateral) resolution are independent. The axial resolution is determined by the coherence length of the source and inversely proportional to the spectral bandwidth. For an optical source with a Gaussian-shaped spectral distribution, the axial resolution Δz is given by

$$\Delta z = \frac{2\ln 2}{\pi} \cdot \frac{\lambda^2}{\Delta\lambda}, \tag{1}$$

where λ is the center wavelength and $\Delta\lambda$ is the spectral bandwidth. To achieve high axial resolution, optical sources with broad spectral bandwidths are desired. Higher resolution could also be achieved by decreasing the center wavelength. However, shorter wavelengths are more highly scattered in biological tissue, resulting in less imaging penetration. A ''biological window'' exists in tissue where light in a range of wavelengths penetrates deep through tissue (Profio & Doiron, 1987). In the near-infrared, roughly between 800 nm and 1,500 nm, light attenuation is more dependent on scattering processes than on absorption processes. At wavelengths below 800 nm, absorption by hemoglobin and melanin dominates light attenuation. At wavelengths above 1,500 nm, light attenuation is mainly due to absorption by water.

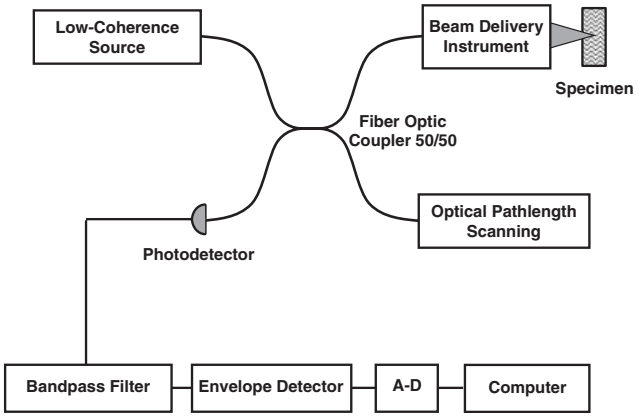

Figure 3. Schematic representation of an OCT system implemented using fiber optics. The Michelson interferometer is implemented using a fiber-optic coupler. Light from the low-coherence source is split and sent to a sample arm with a beam delivery instrument and a reference arm with an optical path length scanner. Reflections from the arms are combined, and the output of the interferometer is detected with a photodiode. The signals are demodulated, processed by a computer, and displayed as an image.

The transverse resolution Δx in an OCT system is determined primarily by the focused spot size, as in conventional microscopy, and is given by

$$\Delta x \approx \frac{4\lambda}{\pi} \cdot \frac{f}{d}, \tag{2}$$

where d is the diameter of the beam size incident on the focusing objective lens and f is its focal length. The incident beam can be focused to a small spot (high transverse resolution) by using optics or an objective with a high numerical aperture. An inherent trade-off exists, however, between spot size and depth of

focus. The depth of focus, as defined by the confocal parameter $2z_R$ (two times the Raleigh range) is given by

$$2z_R = \frac{\pi \Delta x^2}{2\lambda}. \quad (3)$$

Increasing the transverse resolution (smaller Δx) reduces the depth of focus. Commonly, the depth of focus is chosen to match the desired depth of imaging. If higher transverse resolutions are desired, the short depth of focus requires other methods for spatially overlapping the small focal volume with the path-length-matched distances of the reference and sample arms of the interferometer.

The SNR of the OCT system is typically defined as the maximum signal obtained from a perfect reflector (mirror) placed at the focus of the objective in the sample arm, divided by the signal (noise) obtained when one of the arms of the interferometer is blocked. The SNR increases in proportion to the amount of incident optical power and decreases in proportion to the speed at which images are acquired. Laser safety standards (ANSI Z136.1; Laser Institute of America, 2000) limit the maximum optical power that can safety be incident on biological tissue, and these too are dependent on the rate at which the optical beam is scanned across tissue. Imaging within the established laser safety limits, imaging penetration can vary between 1 and 3 mm, depending on the wavelength and the tissue type. Although this depth may initially seem limiting, the majority of pathologies such as cancer originate at mucosal or epithelial surfaces within the imaging depth of OCT. In addition, because the OCT beam can be delivered with a single optical fiber 125 μm in diameter, OCT can be performed deep within biological lumens such as the cardiovascular system (Jang et al., 2002) or the gastrointestinal tract (Das et al., 2001). The small fiber can also be housed within a needle for insertion into solid tissues or suspect masses (Li et al., 2000).

Considerable efforts have been made to increase the speed of OCT image acquisition to reduce the presence of motion artifacts (from patient and physician) and to capture fast dynamic events, such as a beating heart (Boppart, Tearney, et al., 1997; Rollins, et al., 1998) or surgical laser ablation (Boppart et al., 1999, 2001). Image acquisition rates are dependent on the rate at which the reference arm path length can be varied. Typically the acquisition of images 500 × 500 pixels in size can be acquired at several frames per second with a SNR of 100 to 110 dB using 5–10 mW of incident optical power. Optical power requirements can be reduced if lower data acquisition rates and lower SNR can be tolerated.

Technological Developments

Recent developments in OCT technology have been focused on making OCT more useful for diagnostic clinical imaging. These developments include optical sources for high-resolution imaging, fast scanning methods, spectroscopic and Doppler imaging, and digital acquisition and image processing.

The majority of the OCT systems in use today in both research laboratories and in clinical ophthalmology applications utilize a superluminescent diode as a low-coherence light source (Okamoto et al., 1998; Osowski et al., 1994). Superluminescent diodes are commercially available at wavelengths commonly used in the telecommunications industry (800 nm, 1,300 nm, 1,500 nm). These sources are attractive because they are compact, have low electrical power requirements, and low noise. However, their major limitation is low output powers that limit their use to slow image acquisition rates. The available spectral bandwidths are relatively narrow, limiting their imaging resolution to 10–15 μm. Short-pulse femtosecond solid-state lasers are also attractive low-coherence sources for OCT, and have become more user-friendly with their increasing use for multiphoton microscopy (Denk, Strickler, & Webb, 1990; Piston, Kirby, Cheng, Lederer, & Webb, 1994). The titanium:sapphire laser is tunable from 0.7 μm to 1.1 μm and can produce not only broad spectral bandwidths for high-resolution imaging, but also high output powers for fast image acquisition (Bouma et al., 1995; Clivaz, Marquis-Weible, & Salathe, 1992). Recently, titanium:sapphire lasers producing pulses less than two optical cycles in duration with bandwidths as large as 350 nm have been used for ultrahigh axial resolution OCT imaging (Drexler et al., 1999). The chromium:forsterite laser has also been used to generate high output powers and broad spectral bandwidths (5 μm axial resolution) centered around 1,300 nm wavelength, for deeper imaging penetration in highly scattering tissue (Bouma, Tearney, Biliinski, Golubovic, & Fujimoto, 1996). Both of these laser sources, however, are large, require additional pump laser sources, water-cooling, and an experienced operator to align and maintain them. The ultrashort pulses from these lasers can be coupled into new tapered (Birks, Wadsworth, & Russell, 2000), microstructured (Gaeta, 2002), or ultrahigh numerical aperture fiber (Marks, Oldenburg, Reynolds, & Boppart, 2002) to achieve even broader bandwidths and hence higher axial resolution imaging. Supercontinuum spanning wavelengths from approximately 400 to 1,600 nm is possible through nonlinear processes, enabling submicron resolutions (Povazay et al., 2002). Currently, more compact and convenient sources such as superluminescent fiber sources with equivalent optical parameters are currently under investigation (Bashkansky, Duncan, Goldberg, Koplow, & Reintjes, 1998; Paschotta, Nilsson, Tropper, & Hanna, 1997).

The ultrafast solid-state laser sources not only provide broad spectral bandwidth for high-resolution imaging, but also higher output powers for fast real-time OCT imaging. The linear translation of the reference arm mirror is problematic at high rates, limiting axial scan frequencies to approximately 100 Hz, depending on the mirror size and the translating galvanometer or motor. The most commonly used mechanism for performing fast OCT imaging is a phase-controlled optical delay line based on principles used in shaping femtosecond pulses (Tearney, Bouma, & Fujimoto, 1997). This delay line uses a grating to spectrally disperse the beam in the reference arm. The dispersed wavelengths are then focused onto a rotating mirror located at the focus (Fourier transform plane) of a lens. The rotating mirror imparts a wavelength-dependent phase shift on the light. The light then propagates back through the lens and the interferometer. This phase shift in the frequency domain is equivalent to a time delay in the time domain. Practically, it is feasible to pivot a mirror faster than to linearly translate one, and the use of resonantly oscillating scanners to pivot a mirror has enabled axial scan frequencies up to 8 kHz over a scan range of several millimeters. An image with 500 axial scans (columns) can therefore be acquired in 62.5 ms or at a continuous rate of 16 frames per second. High-speed OCT has been used to capture the dynamic motion of a beating *Xenopus laevis* (African frog) tadpole heart and access functional physiologic parameters in response to pharmacologic agents (Boppart, Tearney, et al., 1997; Rollins et al., 1998). The fast acquisition rate also can

capture dynamic processes such as laser ablation for image-guided surgical interventions (Boppart et al., 1999, 2001).

A significant advantage of using light for imaging is the potential to extract spatially distributed spectroscopic data from within the tissue (Leitgeb et al., 2000; Morgner et al., 2000; Schmitt, Xiang, & Yung, 1998). This advantage has clearly been clinically useful in pulse oximetry, where the oxygen saturation of blood is measured by determining the differential absorption spectra at two different wavelengths. Similarly, it should be possible for OCT to spatially map the spectroscopic properties of tissue, such as the oxygenation state of the tissue or regional variations near the surface of the cerebral cortex for monitoring hemodynamic responses to stimuli. In standard OCT, the amplitude of the interference envelope is used to determine the magnitude of the optical backscatter at each position. The full interference signal, however, contains additional information about the local spectroscopic properties as well as information on tissue or scatterer motion that induces a Doppler shift on the returning light. By digitizing the full interference signal and performing digital signal processing using a wavelet or a short-time Fourier transform, spectroscopic data can be extracted from each point within the specimen. An example of spectroscopic imaging in a *Xenopus* tadpole is shown in Figure 4. Although this image indicates changes in the spectroscopic properties of tissue, further investigation is needed to determine how spectroscopic variations in tissue correspond to biological structures and how this additional information can be useful for diagnostic imaging.

In addition to spectroscopic data, transforming the full interference data acquired during OCT scanning can yield information about the motion of scatterers in the tissue, such as blood flow, or the movement of the tissue itself. This technique is called Doppler OCT and has been extensively studied for detecting fluid and blood flow in in vitro models and in vivo tissue (Barton, Welch, & Izatt, 1998; Chen et al., 1997; Izatt, Kulkarni, Yazdanfar, Barton, & Welch, 1997). The sensitivity of this technique is high, enabling the detection of flow rates as slow as 10 μm/s. Techniques such as Doppler OCT would have direct applications in neural imaging for detecting and quantifying localized blood flow within the brain.

As OCT systems become increasingly sophisticated and adapted for clinical use, much of the acquisition and processing of images will need to be done automatically and in real time, behind the user-friendly interface. To facilitate this, almost all of the data management and image processing will be done digitally. Therefore, current research is exploring methods to digitally acquire data and assemble images, incorporating image processing routines that improve resolution and contrast, reduce noise and artifacts, and extract clinically useful image information for making a diagnosis.

Fast digital acquisition and processing can be achieved with the use of digital-signal-processing (DSP) and field-programmable gate array (FPGA) hardware. This hardware enables fast real-time processing with "programmable logic," the ability to interactively program hardware to function as many of the electrical circuits used in analog signal processing. Implementation of this hardware has enabled real-time Doppler imaging of fluid flow within microfluidic tubes (Schaefer, Marks, Reynolds, Balberg, & Boppart, 2001), whereas previous Doppler methods often required longer off-line image-processing time.

Practical clinical OCT systems will require automatic image processing tools for identifying and correcting flaws in OCT images. One type of flaw is the loss of image detail due to the dispersion of the medium. Dispersion occurs because different wavelengths of light propagate at different velocities through tissue. Often in a highly dispersive medium, the axial resolution near the surface is not the same as deeper in the tissue. Dispersion-correction algorithms have been developed to automatically determine the dispersion in the OCT system and throughout all depths of the sample, and to correct for detrimental effects (Marks, Oldenburg, Reynolds, & Boppart, 2003). Previous efforts to compensate dispersion have used digital methods (Fercher et al., 2001) or optical methods (Drexler et al., 1999) to correct the dispersion at one depth in the tissue.

Clinical imaging modalities such as CT, MRI, and US have been established for years, and sophisticated image-processing

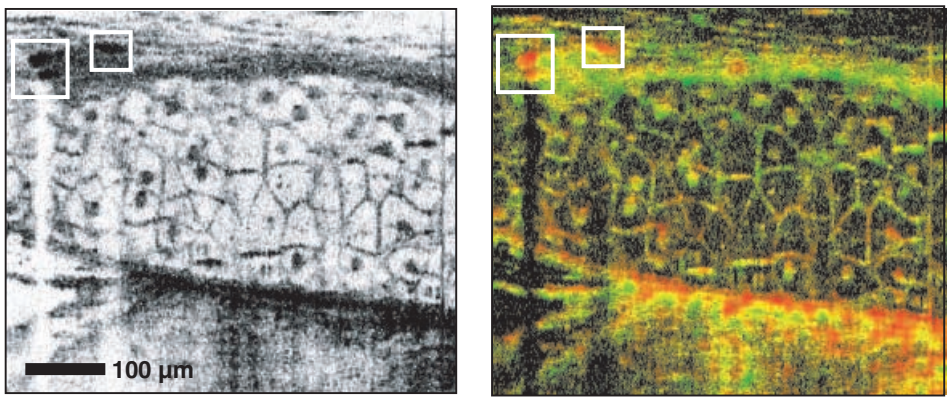

Figure 4. Spectroscopic OCT imaging. Conventional OCT imaging (left) and spectroscopic OCT imaging (right) of in vivo mesenchymal cells in a *Xenopus laevis* (African frog) tadpole. Conventional OCT images represent the optical backscatter intensity, whereas spectroscopic OCT images represent local changes in the absorption or scattering properties of the incident optical spectrum. Melanocytes (boxes) appear red because the melanin within these cells absorb shorter wavelengths of light. The color scale in the spectroscopic image represents the shift of the center of gravity of the optical spectrum for each pixel in the image. Figure reprinted with permission (Morgner et al., 2000).

algorithms have been developed to efficiently extract relevant data. Unlike these modalities, OCT is in its infancy. The unique method by which OCT images are acquired and generated present a new area of investigation for signal and image processing. The flexibility of digital signal and image processing will undoubtedly become an indispensable part of OCT, as it has become for other imaging modalities.

Applications to Neuroimaging

OCT has the potential to provide new imaging, visualization, and quantification capabilities for a wide range of investigations in neuroscience and neuroimaging. Research has demonstrated its potential in the areas of developmental neurobiology, retinal imaging, cellular imaging, brain tumor imaging, and image-guided surgery for the repair of peripheral nerves. Examples of each of these will be described.

In the field of developmental biology, OCT has been demonstrated as a method for performing noninvasive repeated imaging of development in single specimens, without the need for histology at specific time points during development. Imaging studies have been performed on several standard developmental biology animal models including *Rana pipiens* (Leopard frog), *Xenopus laevis* (African frog) (Boppart, Brezinski, Bouma, et al., 1996; Boppart, Brezinski, Tearney, et al., 1996; Boppart, Tearney, et al., 1997), and *Brachydanio rerio* (zebra fish) embryos and eggs (Boppart, Brezinski, Bouma, et al., 1996), the *Mus musculus* (mouse) model (Li, Timmers, Hunter, Gonzalez-Polar, & Lewin, 2001), and *Rattus norvegicus* (rat; Roper et al., 1998).

The developing *Xenopus* central nervous system has been imaged, revealing intricate morphological features at resolutions near that of histology (Boppart, Brezinski, Tearney, et al., 1996). An example of cross-sectional and sagittal imaging of the *Xenopus* brain is shown in Figure 5. These images were acquired from an anesthetized Day 17, Stage 51 tadpole. Structures corresponding to the cerebellum, the medulla oblongata, the choroid plexus, and the olfactory tract can be clearly resolved. Because OCT generates images based on the inherent backscatter from biological tissue, no exogenous fluorophores are necessary, which typically limit specimen viability in fluorescent, confocal, and multiphoton microscopy. Using OCT, extended serial imaging has been performed in zebrafish embryos for up to 48 hr, until hatching, with no observable injury to the specimen (Boppart, Brezinski, Bouma, et al., 1996). Repeated OCT imaging also reduces the need to sacrifice specimens to obtain histological images. This is particularly important in genetic studies, in which genetically modified or mutant specimens can often be limited in availability. Finally, histological processing is costly, time consuming, and difficult on small, fragile specimens. The use of OCT for in vivo imaging reduces many of these disadvantages.

Another in vivo neural imaging study investigated the use of OCT for differentiating normal cortex from experimentally induced cortical dysgenesis in the adult rat neocortex (Roper et al., 1998). Because OCT imaging could not be performed through the intact skull, OCT was performed on exposed cortex and images were compared with corresponding histology. The images produced lacked sufficient contrast to resolve individual cell layers within the cortex, possibly because index changes

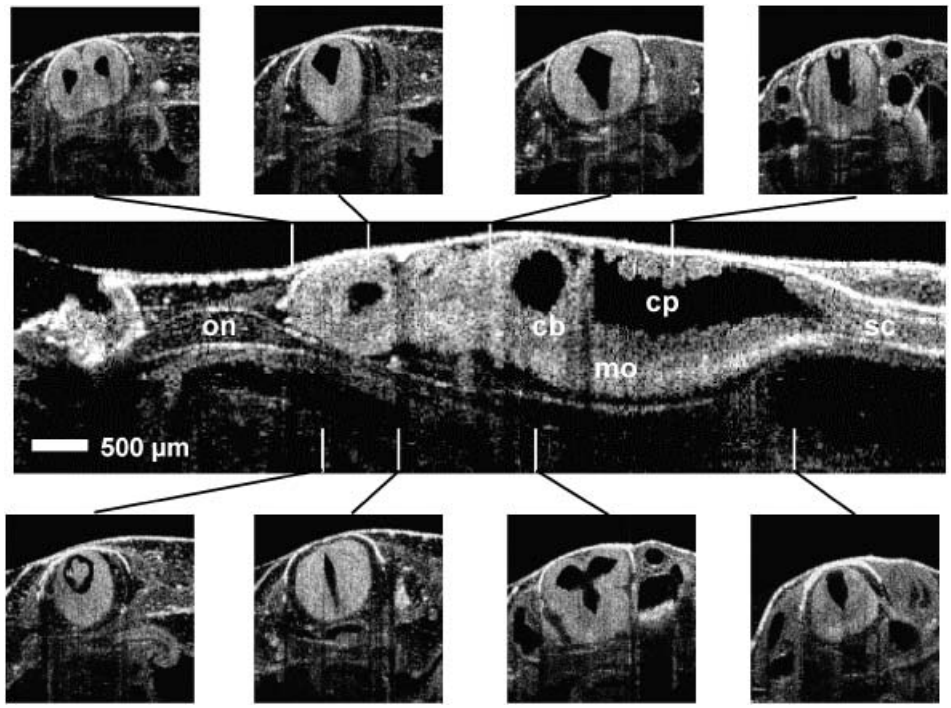

Figure 5. Cross-sectional and sagittal image of the in vivo *Xenopus* brain. Center sagittal image shows structures corresponding to the cerebellum (cb), medulla oblongata (mo), choroid plexus (cp), olfactory tract (ot), and spinal cord (sc). Corresponding cross-sectional images were acquired at various positions along the length of the brain, perpendicular to the anteroposterior axis. Image A shows the paired cerebral hemispheres of the telencephalon and the two lateral ventricles. Image D illustrates the narrowing of the aqueduct of Sylvius connecting the diocoel with the rhombocoel. The posterior choroid plexus, which is on the order of 50–100 μm, is clearly resolved in the fourth ventricle in Image G. Images reprinted with permission (Boppart, Brezinski, Tearney, et al., 1996).

between individual layers were too small. Identifiable structures within the brain included the cortex, subcortical white matter, hippocampus, blood vessels, and the dura mater.

Ophthalmology was the first clinical application for OCT, and subsequently, OCT has become well established in this specialty. OCT of the neural retina at high resolutions has provided images unmatched by any other imaging modality. An example of an ultrahigh resolution image of the human retina is shown in Figure 6. This image was acquired at an axial resolution of 3 μm and a transverse resolution of 15 μm using a titanium:sapphire laser source with exceptionally wide bandwidth. In this image, individual retinal layers can clearly be resolved. The retinal nerve fiber layer, shown as the bright upper band in the retina, characteristically shows thickening in regions closer to the optic disk. Quantification of this nerve fiber layer is important for diagnosing glaucoma and for monitoring the progress of the disease as well as the effectiveness of therapy. The ease at which the neural retina and the retinal vasculature can be accessed offers the potential for using Doppler and spectroscopic OCT techniques to perform hemodynamic functional imaging at this site, providing information on systemic changes that may be occurring.

The high imaging resolutions of OCT enable cellular imaging, and the time-lapse imaging of cellular processes such as mitosis and migration (Boppart, Bouma, Pitris, Southern, et al., 1998). Cellular imaging has been demonstrated in developmental biology animal models primarily because of the high mitotic index, the relatively fast cell movement, and the larger cell sizes of undifferentiated cells. The dynamics of neural crest cell migration is of interest to investigators in developmental neurobiology. The neural crest cells (melanocytes) contain the pigment melanin, providing a natural contrast agent for OCT imaging and facilitating the real-time tracking of migration through a living specimen. A series of three-dimensional (3-D) OCT data sets were obtained from a Day 14, Stage 30 *Xenopus* tadpole at 10-min intervals. From these data sets, cross-sectional images were extracted that contained a neural crest cell. Figure 7 shows the sequence of these cross-sectional images. By referencing the position of this cell to internal morphological features, the position of the cell could be tracked in three dimensions over time. A 3-D plot showing the path of this cell is shown in Figure 8. Techniques such as those illustrated here could be used to track the dynamic behavior of cells in response to developmental, pharmacologic, or genetic interventions.

It is well known that intrinsic optical changes occur in neuronal tissue during cellular physiological events. Shifts in ions, molecules, and water change the local scattering and absorption properties of the tissue. Changes in light scattering have been directly correlated with changes in membrane potential along the axons of single cultured neurons (Stepnoski et al., 1991). Because OCT is sensitive to changes in optical scattering, OCT has the potential to noninvasively detect neural activity without the use of exogenous dyes that would limit the viability of the cells or tissue. Early results from our laboratory have demonstrated that OCT can detect these optical scattering changes in neural tissue.

Imaging cellular processes such as mitosis and migration also have direct relevance to tumor detection and imaging. For example, a significant challenge in neurosurgery is the complete removal of a brain tumor, down to the level of individual cells, while minimizing the complications that result from resecting too wide of margins surrounding the tumor. OCT imaging may provide the resolution and the ability to discriminate tumor cells from normal brain, and do so intraoperatively. OCT has been used to image metastatic melanoma in in vitro human cortex (Boppart, Brezinski, et al., 1998). Examples of OCT images along with corresponding histological images of a metastatic melanoma are shown in Figure 9. Although the melanin present in this metastatic tumor enhanced contrast in the OCT images, it is well known that variations in cell density also change the optical scattering properties of tissue. Therefore, other brain tumors that do not contain melanin but have a higher or lower cell density than normal brain tissue would likely be detectable using OCT.

OCT would be particularly useful intraoperatively for acquiring 3-D volumes of data for the real-time rendering and display of a brain tumor. An example of this capability is shown in Figure 10. The metastatic melanoma tumor shown in Figure 9

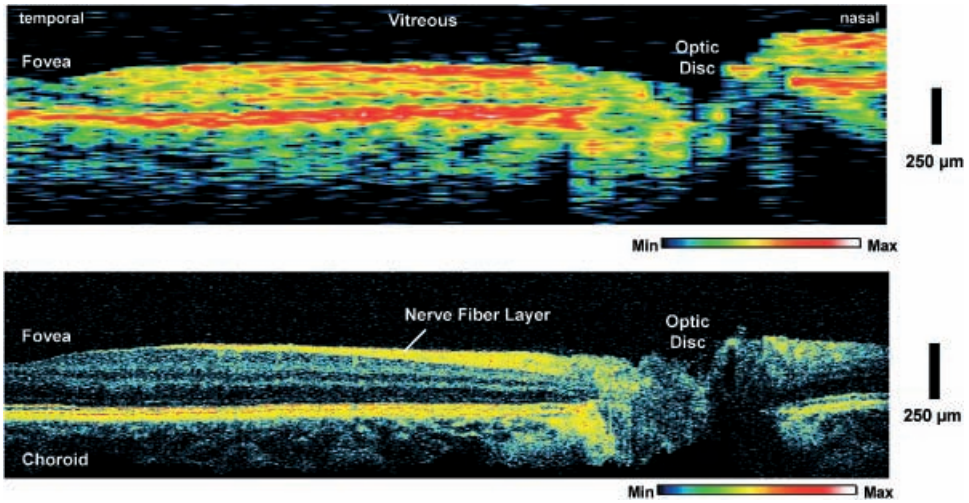

Figure 6. Ultrahigh-resolution image of the human retina. Conventional (top) and ultrahigh-resolution (bottom) in vivo OCT images along the papillomacular axis. Axial resolution is 10 μm (top) and 3 μm (bottom). The nerve fiber layer is well differentiated and varies in thickness between the fovea and the optic disk. Images reprinted with permission (Drexler et al., 2001).

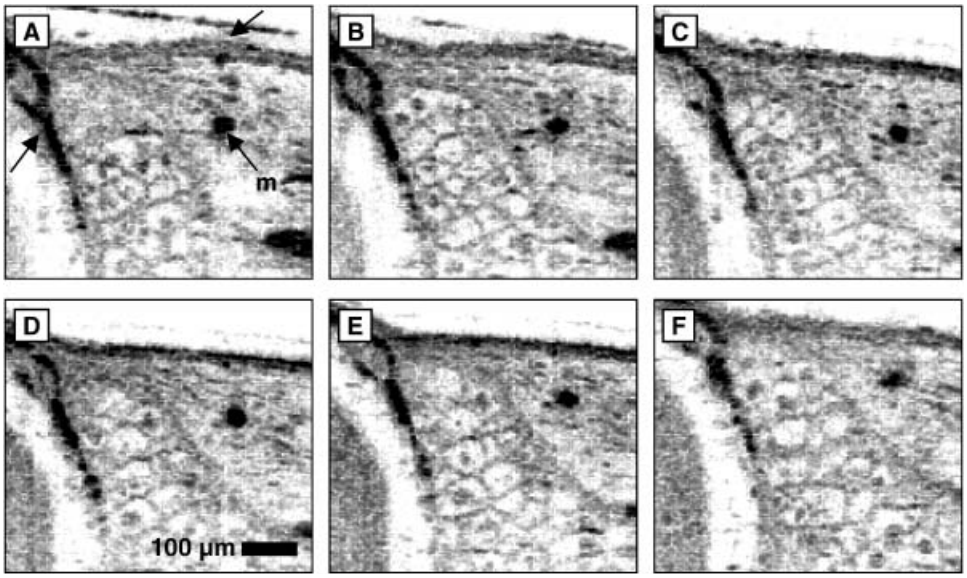

Figure 7. Tracking neural crest cell migration. Image sequence demonstrates in vivo tracking of a neural crest cell (melanocyte, m) through tissue. Position was determined using Cartesian coordinates relative to the outer membrane and melanin layer (black arrows). Three-dimensional volumes of data were acquired at 10-min intervals. Each image represents one section from each 3-D volume. Image reprinted with permission (Boppart, Bouma, Pitris, Tearney, et al., 1998).

was imaged in three dimensions and digitally rendered and displayed for 3-D manipulation and visualization. In contrast to histology, once a 3-D OCT data set is acquired and stored digitally, the volume can be sectioned at arbitrary image planes. In Figure 10, the 3-D data set was resectioned along the *en face* plane, to view images of the tumor as it would be viewed during surgical resection at progressively deeper depths into the brain. The resectioned images show a strong localized signal at 1,200 µm in depth, indicating the possible presence of one or more cells that lie outside of the bulk of the tumor. OCT could possibly be used intraoperatively to image the walls of the cavity created after surgical resection for the presence of residual tumor.

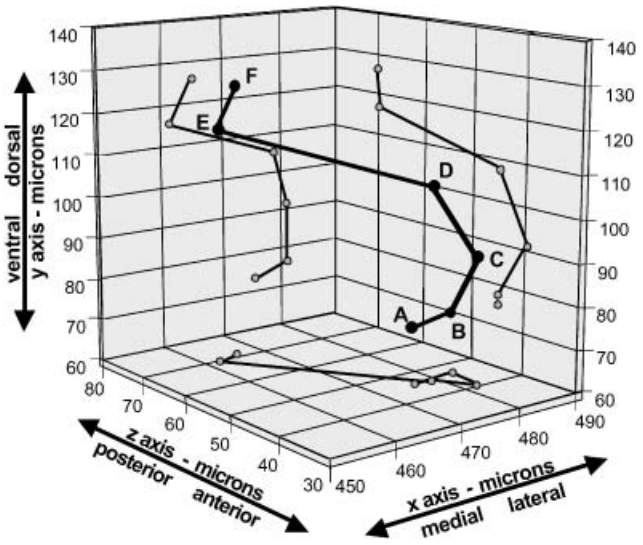

Figure 8. Three-dimensional plot of cell migration. Cell locations were determined from the 3-D data sets acquired for Figure 7. The letter sequence (A–F) corresponds to the position of the cell over time, at 10-min intervals. Projections of the migration are also shown in the transverse, coronal, and sagittal planes. Figure reprinted with permission (Boppart, Bouma, Pitris, Tearney, et al., 1998).

Spectroscopic and Doppler OCT techniques could complement structural OCT imaging of the in vivo human brain. Changes in optical scattering and absorption that occur as a result of neural activity or regional hemodynamic variations can be localized over regions of exposed cerebral cortex. Studies assessing regional changes in microvascular blood flow could be quantified using sensitive Doppler OCT techniques. Unique to these OCT techniques is the ability to spatially resolve changes in three dimensions at resolutions approaching the level of individual cells.

The use of OCT for image-guided surgical applications has been demonstrated for a number of surgically relevant tissues (Boppart et al., 1999, 2001; Boppart, Bouma, Pitris, Tearney, et al., 1998; Brezinski, Tearney, Boppart, et al., 1997). The high-speed subsurface imaging capabilities allow for guiding surgical interventions and for locating blood vessels and nerves (Boppart, Bouma, Pitris, Tearney, et al., 1998). Microsurgical repair of vessels and nerves following traumatic injury is a challenge due to a limited ability to visualize and assess these structures following anastomosis (the reconnection of severed vessels or nerves; Rooks, Slappey, & Zusmanis, 1993). Particularly important in the repair of peripheral nerves is the longitudinal imaging of individual nerve fascicles and the determination of viable, intact nerve (Zhong-wei, Dong-yue, & Di-sheng, 1982). To maximize the possibility for return of function following traumatic nerve injury, individual nerve fascicles must be anastomosed to their corresponding segments. Typically, this is determined by visualization of relative size and position, but can often be ambiguous. Figure 11 is a series of cross-sectional images from a rabbit peripheral nerve showing a single fascicle that has been segmented and highlighted (Boppart, Bouma, Pitris, Tearney, et al., 1998). Included in Figure 11 are projections of the 3-D OCT data set. The longitudinal tracking of individual fascicles revealed a bifurcation in one fascicle, an observation not readily

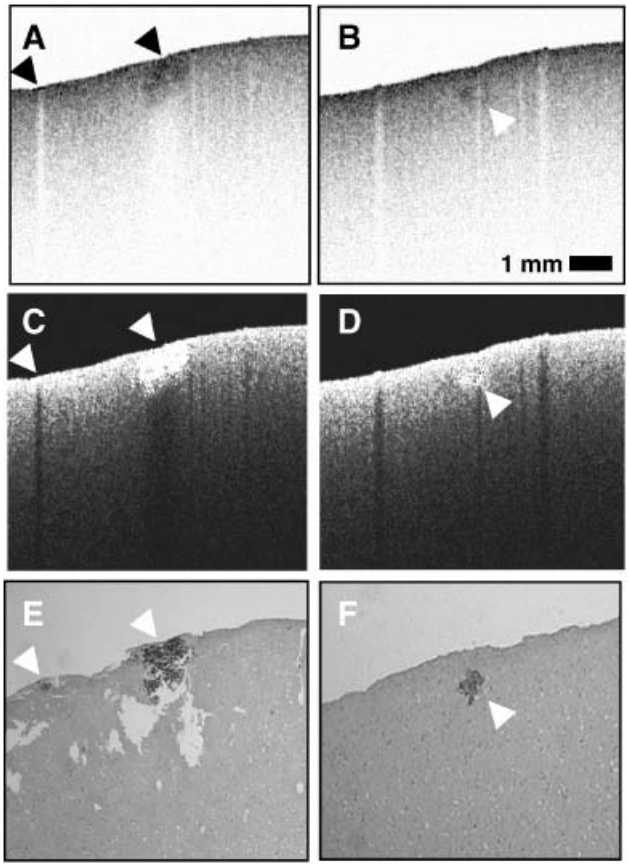

Figure 9. Tumor detection. OCT imaging of malignant melanoma in in vitro human cortical brain tissue. Original OCT images (A,B) were threshold-segmented (C,D) to highlight backscattering tumor. Comparison with corresponding histology (E,F) is strong. The metastatic tumor site in the right column was below the surface and not identified by visual inspection. Images reprinted with permission (Boppart, Brezinski, Pitris, & Fujimoto, 1998).

apparent from viewing single two-dimensional images. Optical scattering changes that occur during excitation of individual neurons will likely be evident in fascicles of nerves and can be detected using OCT. Identifying and quantifying these changes would be useful intraoperatively to assess the viability of injured nerves prior to surgical repair. The use of OCT for quantifying fascicle size, location, longitudinal extent, and viability could possibly improve the outcome following microsurgical repair of severed nerves.

Comparisons with Current Techniques

The realized need for high-resolution real-time functional neuroimaging techniques has prompted investigative efforts to refine MRI, PET, CT, US, and optical imaging modalities for these applications. A number of comparisons and contrasts can be made between OCT and these other imaging modalities. Conventional and Doppler OCT techniques are analogous to B-mode and Doppler US, respectively. OCT, however, has several advantages over US. Because optical wavelengths are shorter than acoustic wavelengths, resolutions as high as 1 μm in tissue can be achieved using OCT, roughly two orders of magnitude higher than conventional US. Although depth of imaging (7–10 mm) is greater for high frequency (~40 MHz)

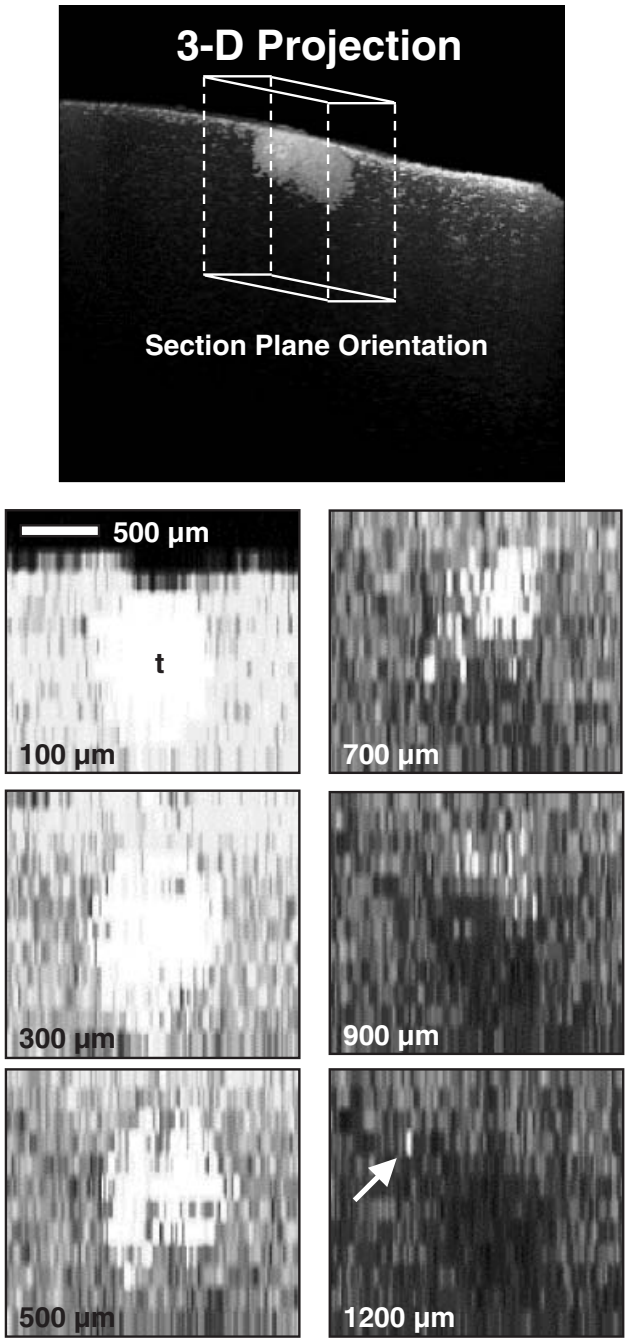

Figure 10. Resectioning of brain tumor. A 3-D OCT data set was acquired from the tumor shown in Figure 9 and resectioned digitally at arbitrary planes on a computer. The top image illustrates the orientation of the planes that were sectioned, parallel to the cortical surface. Sections of the tumor (t) at increasing depths (100–1,200 μm) are shown. A small region of tumor that has penetrated below the central lesion is indicated by the arrow at a depth of 1,200 μm. The dark region shown most prominently at 1,200 μm depth represents shadowing from the central tumor above. Images reprinted with permission (Boppart, Brezinski, Pitris, & Fujimoto, 1998).

US, imaging resolutions were only 30 μm and 90 μm for axial and transverse directions, respectively (Srinivasan et al., 1998). These resolutions do not permit imaging of morphology at the cellular level. In contrast to US, OCT imaging is noncontact and can be

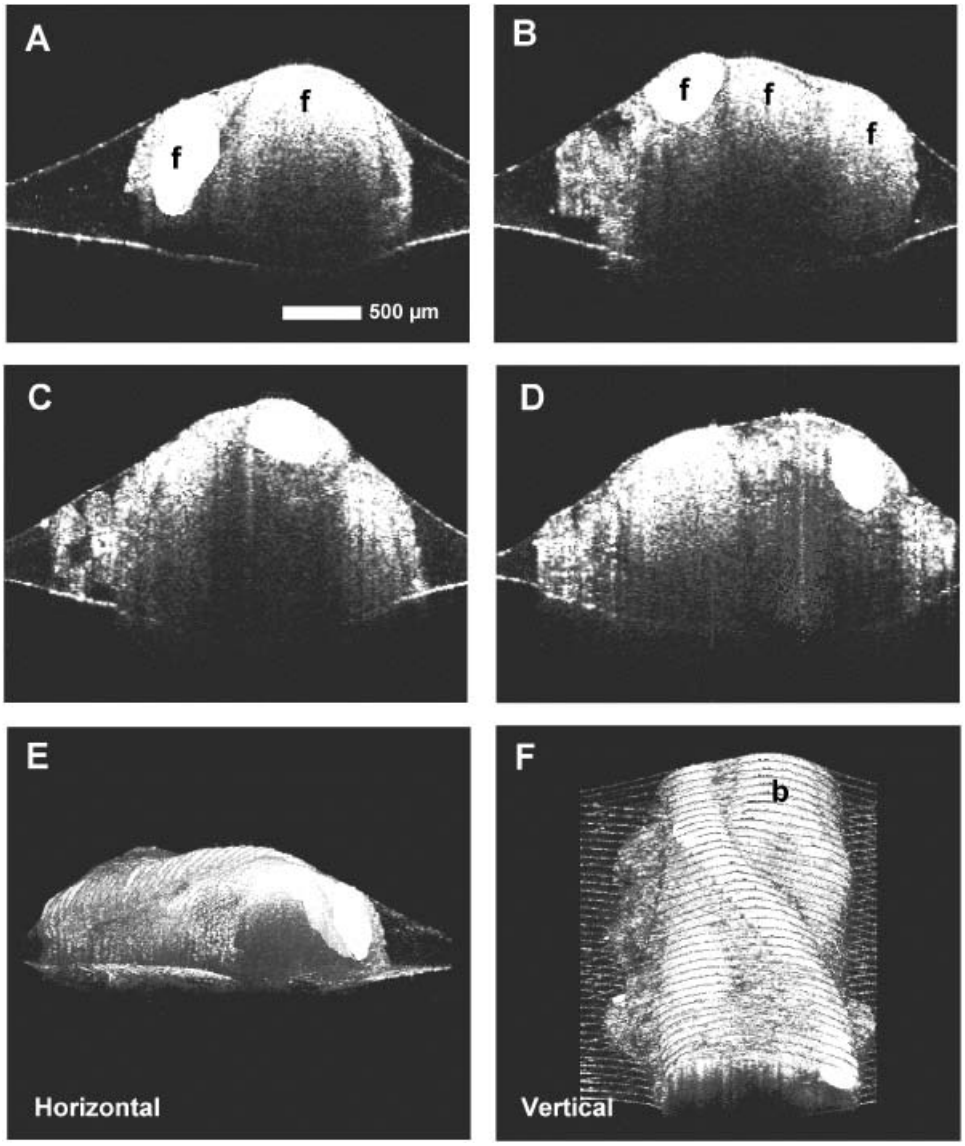

Figure 11. Microsurgical OCT image-guidance of nerve anastomosis. Three-dimensional OCT imaging of a peripheral nerve reveals multiple fascicles (f). A single fascicle was followed longitudinally along the axis of the nerve, manually segmented, and colored white (A–D). Horizontally (E) and vertically (F) oriented 3-D projections illustrate the spatial arrangement of individual fascicles and a bifurcation (b) that was not previously appreciated in two-dimensional cross sections. Images reprinted with permission (Boppart, Bouma, Pitris, Tearney, Southern, et al., 1998).

performed through air, eliminating the need for the index-matching fluids or gels. Because light can be easily delivered using small optical fibers, the imaging "transducer" can be located remote from the specimen. Ultrahigh frequency ($\sim$120 MHz) US transducers have been fabricated on needle-based probes for in vivo imaging, providing 23-μm axial and 13-μm transverse resolution (Yokosawa et al., 2000). These needle probes have been used to image and differentiate renal structures in a living mouse. Higher-resolution US imaging, however, comes at the expense of a further decreased depth of field (81 μm for the needle probe; Yokosawa et al., 2000). The depth to which OCT can image is dependent on the optical properties of the tissue. In highly scattering tissue such as skin or muscle, imaging penetration is 2–3 mm. In more transparent structures such as the eye, imaging depths of 10–20 mm are feasible, with micron-scale resolution. Both OCT and US can image in real time (16–32 frames per second). Because of the spectral properties of tissue, optical spectroscopy can be used to obtain additional image data from cells and tissue.

Well-recognized imaging technologies for structural and functional neuroimaging include MRI, PET, and CT. These modalities have been developed for in vivo neuroimaging in humans, but frequently require large, expensive, and complex systems. For these modalities, a trade-off exists between imaging large structures such as the brain at the expense of high cellular-level resolution. Although investigators are improving the resolution of these clinical modalities, the acquisition of large 3-D data sets requires lengthy acquisition times to yield data with high signal to noise. An opportunity therefore exists to integrate multiple imaging modalities to address this large range of scale and future studies will likely include complementary data, for example, from functional brain MRI and high-resolution optical imaging techniques.

Comparisons can also be made between OCT and other optical microscopy techniques. Multiphoton microscopy has been clearly shown to improve imaging resolution and depth of imaging compared to fluorescent and reflectance confocal microscopy (Denk et al., 1990; So, Kim, & Kochevar, 1998; Piston et al., 1994). The use of near-infrared wavelengths permits deeper tissue imaging (200–300 μm) and less tissue damage compared to visible laser wavelengths. Beam delivery and optical systems for performing multiphoton microscopy at remote sites is problematic, and current research is investigating methods for performing these techniques using fiber-optic delivery. Confocal microscopy utilizes the spatial rejection of out-of-focus light to improve resolution and contrast. In a similar manner, the single-mode optical fiber used in OCT serves an analogous function as the pinhole in confocal microscopy, as a spatial filter of the light. In addition, the coherence detection of OCT can reject light present at the focal plane that may have been multiply scattered from elsewhere in the tissue. Hence, the combination of OCT and confocal microscopy can improve the depth of imaging over confocal microscopy alone. Although fluorescent-based techniques can provide site-specific targeting for probes to cells and tissues, the administration of exogenous contrast agents requires additional safety screening for their use, particularly as excitation of fluorescent probes can produce cytotoxic byproducts. Because OCT relies on inherent optical scattering properties of tissue, images can be generated without the use of exogenous contrast agents.

Whereas OCT and optical microscopy techniques rely on backscattered or fluorescent light collected within a focal volume, the field of diffusion optical imaging relies on the collection of multiply scattered diffusing photons that have traveled relatively large distances through tissue (Strangman, Boas, & Sutton, 2002; Villringer & Chance, 1997). Typically delivery and collection fibers are arranged geometrically around the tissue (typically the head or breast) and images are generated based on the collected light from each fiber. Although the penetration depth for near-infrared light in tissue can be several centimeters, the spatial resolution of these tomographic techniques is low, typically on the order of several millimeters. Still, because these optical techniques are more portable and less expensive than MRI or PET, and because information on the hemodynamic state of the tissue can be extracted, these diffusion-based optical techniques are attractive for noninvasive imaging in humans.

Conclusions

Since its inception in the early 1990s, the OCT technology and its applications have extended across many medical, biological, and nonbiological fields. Despite the rapid development and implementation of this technology, relatively few applications have been in the fields of neuroscience and neuroimaging. This can most likely be attributed to the relatively recent development of this technology and its broad application across multiple fields. The highly scattering neural tissue of the central and peripheral nervous system can appear somewhat homogeneous in OCT images, providing a challenge to extract microstructural or functional information from the image data. The use of spectroscopic and Doppler OCT can provide additional image contrast mechanisms to differentiate structure and assess functional activity. Because the imaging penetration of OCT is limited to a few millimeters, initial in vivo human studies will likely be limited to open surgical procedures that expose neural tissue. However, the fiber-based delivery of the OCT beam can provide a means for minimally invasive imaging procedures or for the use of implanted optical fibers for long-term data collection. Despite these challenges, the noninvasive, high-resolution, real-time imaging capabilities of OCT make it an attractive investigational tool for imaging tissue morphology, monitoring cellular dynamics, and mapping molecular (spectroscopic) properties.

Future technological advancements are likely to be in the areas of new compact and portable optical sources, new digital signal and image processing algorithms, and methods to extract clinically useful information from acquired data. Future applications in neuroscience and neural imaging include tracking the dynamic processes in the neural development of normal and genetically modified animal models, investigating the dynamic processes of cell migration in both development and tumorgenesis, the use of spectroscopic and Doppler OCT techniques for determining the spatial distribution of neural activity, blood flow, and oxygenation states, and for intraoperative image-guided surgical procedures involving the central and peripheral nervous systems. In time, it is expected that diagnostic OCT imaging will become standard practice in a wide range of medical and surgical specialties, just as CT, MRI, PET, and US are today.

REFERENCES

Barton, J. K., Welch, A. J., & Izatt, J. A. (1998). Investigating pulsed dye laser-blood vessel interaction with color Doppler optical coherence tomography. *Optics Express*, *3*, 251–256.

Bashkansky, M., Duncan, M. D., Goldberg, L., Koplow, J. P., & Reintjes, J. (1998). Characteristics of a Yb-doped superfluorescent fiber source for use in optical coherence tomography. *Optics Express*, *3*, 305–310.

Beaurepaire, E., Moreaux, L., Amblard, F., & Mertz, J. (1999). Combined scanning optical coherence and two-photon-excited fluorescence microscopy. *Optics Letters*, *24*, 969–971.

Birks, T. A., Wadsworth, W. J., & Russell, P. S. J. (2000). Supercontinuum generation in tapered fibers. *Optics Letters*, *25*, 1415–1417.

Boppart, S. A., Bouma, B. E., Pitris, C., Southern, J. F., Brezinski, M. E., & Fujimoto, J. G. (1998). In vivo cellular optical coherence tomography imaging. *Nature Medicine*, *4*, 861–864.

Boppart, S. A., Bouma, B. E., Pitris, C., Tearney, G. J., Fujimoto, J. G., & Brezinski, M. E. (1997). Forward-scanning instruments for optical coherence tomographic imaging. *Optics Letters*, *22*, 1618–1620.

Boppart, S. A., Bouma, B. E., Pitris, C., Tearney, G. J., Southern, J. F., Brezinski, M. E., & Fujimoto, J. G. (1998). Intraoperative assessment of microsurgery with three-dimensional optical coherence tomography. *Radiology*, *208*, 81–86.

Boppart, S. A., Brezinski, M. E., Bouma, B. E., Tearney, G. J., & Fujimoto, J. G. (1996). Investigation of developing embryonic morphology using optical coherence tomography. *Developmental Biology*, *177*, 54–63.

Boppart, S. A., Brezinski, M. E., Pitris, C., & Fujimoto, J. G. (1998). Optical coherence tomography for neurosurgical imaging of intracortical melanoma. *Neurosurgery*, *43*, 834–841.

Boppart, S. A., Brezinski, M. E., Tearney, G. J., Bouma, B. E., & Fujimoto, J. G. (1996). Imaging developing neural morphology using optical coherence tomography. *Journal of Neuroscience Methods*, *2112*, 65–72.

Boppart, S. A., Herrmann, J. M., Pitris, C., Stamper, D. L., Brezinski, M. E., & Fujimoto, J. G. (1999). High-resolution optical coherence tomography guided laser ablation of surgical tissue. *Journal of Surgical Research*, *82*, 275–284.

Boppart, S. A., Herrmann, J. M., Pitris, C., Stamper, D. L., Brezinski, M. E., & Fujimoto, J. G. (2001). Real-time optical coherence tomography for minimally invasive imaging of prostate ablation. *Computer Aided Surgery*, *6*, 94–103.

Boppart, S. A., Tearney, G. J., Bouma, B. E., Southern, J. F., Brezinski, M. E., & Fujimoto, J. G. (1997). Noninvasive assessment of the developing *Xenopus* cardiovascular system using optical coherence tomography. *Proceedings of the National Academy of Sciences, USA*, *94*, 4256–4261.

Bouma, B. E., & Tearney G. J. (Eds.) (2001). *Handbook of Optical Coherence Tomography*. New York: Marcel Dekker, Inc.

Bouma, B. E., Tearney, G. J., Biliinski, I. P., Golubovic, B., & Fujimoto, J. G. (1996). Self-phase-modulated Kerr-lens mode-locked Cr: foorsterite laser source for optical coherence tomography. *Optics Letters*, *21*, 1839–1842.

Bouma, B. E., Tearney, G. J., Boppart, S. A., Hee, M. R., Brezinski, M. E., & Fujimoto, J. G. (1995). High-resolution optical coherence tomographic imaging using a mode-locked Ti: Al_2O_3 laser source. *Optics Letters*, *20*, 1486–1489.

Bouma, B. E., Tearney, G. J., Compton, C. C., & Nishioka, N. S. (2000). High-resolution imaging of the human esophagus and stomach in vivo using optical coherence tomography. *Gastrointestinal Endoscopy*, *51*(4 Pt 1), 467–474.

Bowd, C., Zangwill, L. M., Berry, C. C., Blumenthal, E. Z., Vasile, C., Sanchez-Galeana, C., Bosworth, C. F., Sample, P. A., & Weinreb, R. N. (2001). Detecting early glaucoma by assessment of retinal nerve fiber layer thickness and visual function. *Investigative Ophthalmology & Visual Science*, *42*, 1993–2003.

Brezinski, M. E., Tearney, G. J., Boppart, S. A., Swanson, E. A., Southern, J. F., & Fujimoto, J. G. (1997). Optical biopsy with optical coherence tomography, feasibility for surgical diagnostics. *Journal of Surgical Research*, *71*, 32–40.

Brezinski, M. E., Tearney, G. J., Bouma, B. E., Izatt, J. A., Hee, M. R., Swanson, E. A., Southern, J. F., & Fujimoto, J. G. (1996). Optical coherence tomography for optical biopsy: Properties and demonstration of vascular pathology. *Circulation*, *93*, 1206–1213.

Brezinski, M. E., Tearney, G. J., Weissman, N. J., Boppart, S. A., Bouma, B. E., Hee, M. R., Weyman, A. E., Swanson, E. A., Southern, J. F., & Fujimoto, J. G. (1997). Assessing atherosclerotic plaque morphology: Comparison of optical coherence tomography and high frequency intravascular ultrasound. *British Heart Journal*, *77*, 397–404.

Chen, Z., Milner, T. E., Srinivas, S., Wang, X., Malekafzali, A., van Germert, M. J. C., & Nelson, J. S. (1997). Noninvasive imaging of in vivo blood flow velocity using optical Doppler tomography. *Optics Letters*, *22*, 1119–1120.

Chinn, S. R., & Swanson, E. A. (1996). Multilayer optical storage by low-coherence reflectometry. *Optics Letters*, *21*, 899–901.

Clivaz, X., Marquis-Weible, F., & Salathe, R. P. (1992). Optical low coherence reflectometry with 1.9 μm spatial resolution. *Electronics Letters*, *28*, 1553–1555.

Colston, B. W., Jr., Everett, M. J., Da Silva, L. B., Otis, L. L., Stroeve, P., & Nathal, H. (1998). Imaging of hard- and soft-tissue structure in the oral cavity by optical coherence tomography. *Applied Optics*, *37*, 3582–3585.

Das, A., Sivak, M. V., Jr., Chak, A., Wong, R. C., Westphal, V., Rollins, A. M., Willis, J., Isenberg, G., & Izatt, J. A. (2001). High-resolution endoscopic imaging of the GI tract: A comparative study of optical coherence tomography versus high-frequency catheter probe EUS. *Gastrointestinal Endoscopy*, *54*, 219–224.

Denk, W., Strickler, J. H., & Webb, W. W. (1990). Two-photon laser scanning fluorescence microscopy. *Science*, *248*, 73–76.

Drexler, W., Morgner, U., Ghanta, R. K., Kartner, F. X., Schuman, J. S., & Fujimoto, J. G. (2001). Ultrahigh resolution ophthalmic optical coherence tomography. *Nature Medicine*, *7*, 502–507.

Drexler, W., Morgner, U., Kartner, F. X., Pitris, C., Boppart, S. A., Li, X. D., Ippen, E. P., & Fujimoto, J. G. (1999). In vivo ultrahigh-reso-lution optical coherence tomography. *Optics Letters*, *24*, 1221–1223.

Duncan, M. D., Bashkansky, M., & Reintjes, J. (1998). Subsurface defect detection in materials using optical coherence tomography. *Optics Express*, *2*, 540–545.

Feidchtein, F. I., Gelikonov, G. V., Gelikonov, V. M., Kuranov, R. V., Sergeev, A. M., Gladkova, N. D., Shakhov, A. V., Shakhova, N. M., Snopova, L. B., Terent'eva, A. B., Zagainova, E. V., Chumakov, Yu. P., & Kuznetzova, I. A. (1998). Endoscopic applications of optical coherence tomography. *Optics Express*, *3*, 257–270.

Fercher, A. F., Hitzenberger, C. K., Sticker, M., Zawadski, R., Karamata, B., & Lasser, T. (2001). Numerical dispersion compensation for partial coherence interferometry and optical coherence tomography. *Optics Express*, *9*, 610–615.

Fercher, A. F., Mengedoht, K., & Werner, W. (1988). Eye-length measurement by interferometry with partially coherent light. *Optics Letters*, *13*, 186–190.

Fujimoto, J. G., Pitris, C., Boppart, S. A., & Brezinski, M. E. (2000). Optical coherence tomography: An emerging technology for biomedical imaging and optical biopsy. *Neoplasia*, *2*, 9–25.

Gaeta, A. L. (2002). Nonlinear propagation and continuum generation in microstructured optical fibers. *Optics Letters*, *27*, 924–926.

Hee, M. R., Izatt, J. A., Swanson, E. A., Huang, D., Schuman, J. S., Lin, C. P., Puliafito, C. A., & Fujimoto, J. G. (1995). Optical coherence tomography of the human retina. *Archives of Ophthalmology*, *113*, 325–332.

Hitzenberger, C. K. (1991). Measurement of the axial eye length by laser Doppler interferometry. *Investigative Ophthalmology & Visual Science*, *32*, 616–624.

Huang, D., Swanson, E. A., Lin, C. P., Schuman, J. S., Stinson, W. G., Chang, W., Hee, M. R., Flotte, T., Gregory, K., Puliafito, C. A., & Fujimoto, J. G. (1991). Optical coherence tomography. *Science*, *254*, 1178–1181.

Izatt, J. A., Kulkarni, M. D., Wang, H.-W., Kobayashi, K., & Sivak, M. V. (1996). Optical coherence tomography and microscopy in gastrointestinal tissues. *IEEE Journal of Selected Topics in Quantum Electronics*, *2*, 1017–1028.

Izatt, J. A., Kulkarni, M. D., Yazdanfar, S., Barton, J. K., & Welch, A. J. (1997). In vivo bidirectional color doppler flow imaging of picoliter blood volumes using optical coherence tomography. *Optics Letters*, *22*, 1439–1441.

Jang, I. K., Bouma, B. E., Kang, D. H., Park, S. J., Park, S. W., Seung, K. B., Choi, K. B., Shishkov, M., Schlendorf, K., Pomerantsev, E., Houser, S. L., Aretz, H. T., & Tearney, G. J. (2002). Visualization of coronary atherosclerosis plaques in patients using optical coherence tomography: comparison with intravascular ultrasound. *Journal of the American College of Cardiology*, *39*, 604–609.

Laser Institute of America. (2000). *American National Standard for the Safe Use of Lasers*, ANSI Z136.1. Orlando, FL: Author.

Leitgeb, R., Wojtkowski, M., Kowalczyk, A., Hitzenberger, C. K., Sticker, M., & Fercher, A. F. (2000). Spectral measurement of absorption by spectroscopic frequency-domain optical coherence tomography. *Optics Letters*, *25*, 820–822.

Li, Q., Timmers, A. M., Hunter, K., Gonzalez-Pola, C., & Lewin, A. S. (2001). Noninvasive imaging by optical coherence tomography to monitor retinal degeneration in the mouse. *Investigative Ophthalmology & Visual Science*, *42*, 2981–2989.

Li, X., Chudoba, C., Ko, T., Pitris, C., & Fujimoto, J. G. (2000). Imaging needle for optical coherence tomography. *Optics Letters*, *25*, 1520–1522.

Li, X. D., Boppart, S. A., Van Dam, J., Mashimo, H., Mutinga, M., Drexler, W., Klein, M., Pitris, C., Krinsky, M. L., Brezinski, M. E., & Fujimoto, J. G. (2001). Optical coherence tomography: Advanced technology for the endoscopic imaging of Barrett's esophagus. *Endoscopy*, *32*, 921–930.

Marks, D. L., Oldenburg, A. L., Reynolds, J. J., & Boppart, S. A. (2002). Study of an ultrahigh numerical aperture fiber continuum generation source for optical coherence tomography. *Optics Letters*, *27*, 2010–2012.

Marks, D. L., Oldenburg, A. L., Reynolds, J. J., & Boppart, S. A. (2003). Digital algorithm for dispersion correction in optical coherence tomography for homogeneous and stratified media. *Applied Optics*, *42*, 204–217.

Morgner, U., Drexler, W., Kartner, F. X., Li, X. D., Pitris, C., Ippen, E. P., & Fujimoto, J. G. (2000). Spectroscopic optical coherence tomography. *Optics Letters*, *25*, 111–113.

Okamoto, H., Wada, M., Sakai, Y., Hirono, T., Kawaguchi, Y., Kondo, Y., Kadota, Y., Kishi, K., & Itaya, Y. (1998). A narrow beam 1.3 micrometer superluminescent diode integrated with a spot-size converter and a new type rear absorbing region. *Journal of Lightwave Technology*, *16*, 1881–1887.

Osowski, M. L., Cockerill, T. M., Lammert, R. M., Forbes, D. V., Ackley, D. E., & Coleman, J. J. (1994). A strained-layer InGaAs-

GaAs-AlGaAs single quantum well broad spectrum LED by selective-area metalorganic chemical vapor deposition. *IEEE Photonics Technology Letters*, *6*, 1289–1292.

Pan, Y., Xie, H., & Fedder, G. K. (2001). Endoscopic optical coherence tomography based on a microelectromechanical mirror. *Optics Letters*, *26*, 1966–1969.

Paschotta, R., Nilsson, J., Tropper, A. C., & Hanna, D. C. (1997). Efficient superfluorescent light sources with broad bandwidth. *IEEE Journal of Selected Topics in Quantum Electronics*, *3*, 1097–1099.

Piston, D. W., Kirby, M. S., Cheng, H., Lederer, W. J., & Webb, W. W. (1994). Two-photon-excitation fluorescence imaging of three-dimensional calcium-ion activity. *Applied Optics*, *33*, 662–669.

Podoleanu, A. G., Rogers, J. A., Jackson, D. A., & Dunne, S. (2000). Three dimensional OCT images from retina and skin. *Optics Express*, *7*, 292–298.

Povazay, B., Bizheva, K., Unterhuber, A., Hermann, B., Sattmann, H., Fercher, A. F., Drexler, W., Apolonski, A., Wadsworth, W. J., Knight, J. C., Russell, P. S. J., Vetterlein, M., & Scherzer, E. (2002). Submicrometer axial resolution optical coherence tomography. *Optics Letters*, *27*, 1800–1802.

Profio, A. E., & Doiron, D. R. (1987). Transport of light in tissue in photodynamic therapy. *Photochemistry and Photobiology*, *46*, 591–599.

Puliafito, C. A., Hee, M. R., Lin, C. P., Reichel, E., Schuman, J. S., Duker, J. S., Izatt, J. A., Swanson, E. A., & Fujimoto, J. G. (1995). Imaging of macular disease with optical coherence tomography (OCT). *Ophthalmology*, *102*, 217–229.

Puliafito, C. A., Hee, M. R., Schuman, J. S., & Fujimoto, J. G. (1995). *Optical coherence tomography of ocular diseases*. Thorofare, NJ: Slack, Inc.

Rollins, A. M., Kulkarni, M. D., Yazdanfar, S., Ung-arunyawee, R., & Izatt, J. A. (1998). In vivo video rate optical coherence tomography. *Optics Express*, *3*, 219–229.

Rooks, M. D., Slappey, J., & Zusmanis, K. (1993). Precision of suture placement with microscope- and loupe-assisted anastomoses. *Microsurgery*, *14*, 547–550.

Roper, S. N., Moores, M. D., Gelikonov, G. V., Feldchtein, F. I., Beach, N. M., King, M. A., Gelikonov, V. M., Sergeev, A. M., & Reitze, D. H. (1998). In vivo detection of experimentally induced cortical dysgenesis in the adult rat neocortex using optical coherence tomography. *Journal of Neuroscience Methods*, *80*, 91–98.

Schaefer, A. W., Marks, D. L., Reynolds, J. J., Balberg, M., & Boppart, S. A. (2001). Real-time DSP-based optical Doppler tomography for analyzing microfluidic bioMEM devices. Paper WV2 presented at the Optical Society of America Annual Meeting.

Schmitt, J. M., Xiang, S. H., & Yung, K. M. (1998). Differential absorption imaging with optical coherence tomography. *Journal of the Optical Society of America A*, *15*, 2288–2296.

Schmitt, J. M., Yadlowsky, M. J., & Bonner, R. F. (1995). Subsurface imaging of living skin with optical coherence microscopy. *Dermatology*, *191*, 93–98.

So, P. T. C., Kim, H., & Kochevar, I. E. (1998). Two-photon deep tissue ex vivo imaging of mouse dermal and subcutaneous structures. *Optics Express*, *3*, 339–350.

Srinivasan, S., Baldwin, H. S., Aristizabal, O., Kwee, L., Labow, M., Artman, M., & Turnbull, D. H. (1998). Noninvasive, in utero imaging of mouse embryonic heart development with 40-MHz echocardiography. *Circulation*, *98*, 912–918.

Stepnoski, R. A., LaPorta, A., Raccuia-Behling, F., Blonder, G. E., Slusher, R. E., & Kleinfeld, D. (1991). Noninvasive detection of changes in membrane potential in cultured neurons by light scattering. *Proceedings of the National Academy of Sciences, USA*, *88*, 9382–9386.

Strangman, G., Boas, D. A., & Sutton, J. P. (2002). Non-invasive neuroimaging using near-infrared light. *Biological Psychiarty*, *52*, 679–693.

Takada, K., Yokohama, I., Chida, K., & Noda, J. (1987). New measurement system for fault location in optical waveguide devices based on an interferometric technique. *Applied Optics*, *26*, 1603–1606.

Tearney, G. J., Bouma, B. E., & Fujimoto, J. G. (1997). High-speed phase- and group-delay scanning with a grating-based phase control delay line. *Optics Letters*, *22*, 1811–1813.

Tearney, G. J., Brezinski, M. E., Boppart, S. A., Bouma, B. E., Weissman, N., Southern, J. F., Swanson , E. A., & Fujimoto, J. G. (1996). Catheter-based optical imaging of a human coronary artery. *Circulation*, *94*, 3013.

Tearney, G. J., Brezinski, M. E., Bouma, B. E., Boppart, S. A., Pitris, C., Southern, J. F., & Fujimoto, J. G. (1997). In vivo endoscopic optical biopsy with optical coherence tomography. *Science*, *276*, 2037–2039.

Tearney, G. J., Brezinski, M. E., Southern, J. F., Bouma, B. E., Boppart, S. A., & Fujimoto, J. G. (1997a). Optical biopsy in human gastrointestinal tissue using optical coherence tomography. *American Journal of Gastroenterology*, *92*, 1800–1804.

Tearney, G. J., Brezinski, M. E., Southern, J. F., Bouma, B. E., Boppart, S. A., & Fujimoto, J. G. (1997b). Optical biopsy in human urologic tissue using optical coherence tomography. *Journal of Urology*, *157*, 1915–1919.

Villringer, A., & Chance, B. (1997). Non-invasive optical spectroscopy and imaging of human brain function. *Trends in Neurosciences*, *20*, 435–442.

Williams, Z. Y., Schuman, J. S., Gamell, L., Nemi, A., Hertzmark, E., Fujimoto, J. G., Mattox, C., Simpson, J., & Wollstein, G. (2002). Optical coherence tomography measurement of nerve fiber layer thickness and the likelihood of a visual field defect. *American Journal of Ophthalmology*, *134*, 538–546.

Xu, F., Pudavar, H. E., Prasad, P. N., & Dickensheets, D. (1999). Confocal enhanced optical coherence tomography for non-destructive evaluation of paints and coatings. *Optics Letters*, *24*, 1808–1810.

Yokosawa, K., Sasaki, D., Umemura, S.-I., Shinomura, R., Ishikawa, S., Sano, S., & Ito, Y. (2000). Intracorporeal imaging and differentiation of living tissue with an ultra-high-frequency ultrasound probe. *Ultrasound in Medicine and Biology*, *26*, 503–507.

Zagaynova, E. V., Streltsova, O. S., Gladkova, N. D., Snopova, L. B., Gelikonov, G. V., Feldchtein, F. I., & Morozov, A. N. (2001). In vivo optical coherence tomography feasibility for bladder disease. *Journal of Urology*, *167*, 1492–1496.

Zhong-wei, C., Dong-yue, Y., & Di-Sheng, C. (Eds.). (1982). *Microsurgery*. New York: Springer Verlag.

(Received July 5, 2002; Accepted November 24, 2002)